

Two Types of Mixed Orthogonal Frequency Division Multiplexing (X-OFDM) Waveform for Optical Wireless Communication

Xu Li, Jingjing Huang, Yibo Lyu, Rui Ni, Jiajin Luo, Junping Zhang

Abstract—The optical wireless communication (OWC) with the intensity modulation (IM), requires the modulated radio frequency (RF) signal to be real and non-negative. To satisfy the requirements, this paper proposes two types of mixed orthogonal frequency division multiplexing (X-OFDM) waveform. The Hermitian symmetry (HS) character of the sub-carriers in the frequency domain, guarantees the signal in the time domain to be real, which reduces the spectral efficiency to $1/2$. For the odd sub-carriers in the frequency domain, the signal in the time domain after the inverse fast fourier transform (IFFT) is antisymmetric. For the even sub-carriers in the frequency domain, the signal in the time domain after the IFFT is symmetric. Based on the antisymmetric and symmetric characters, the two types of X-OFDM waveform are designed to guarantee the signal in the time domain to be non-negative, where the direct current (DC) bias is not needed. With N sub-carriers in the frequency domain, the generated signal in the time domain has $3N/2$ points, which further reduces the spectral efficiency to $1/3 = 1/2 \times 2/3$. The numerical simulations show that, the two types of X-OFDM waveform greatly enhance the power efficiency considering the OWC channel with the signal-dependent noise and/or the signal-independent noise.

Index Terms—Optical wireless communication (OWC), Intensity Modulation (IM), Mixed Orthogonal Frequency Division Multiplexing (X-OFDM) Waveform, Peak to Average Power Ratio (PAPR), Bit Error Rate (BER), Power Efficiency

I. INTRODUCTION

The optical wireless communication (OWC) is a candidate technology for the communication beyond fifth-generation (5G), to provide the services with ultra-high system capacity, ultra-low latency, ultra-high security, ultra-low energy consumption, and etc. [1]. Differs from the wireless radio frequency (RF) band between 3kHz and 300GHz of the electromagnetic spectrum, the wireless connectivity based on the optical spectrum is termed as the OWC [2].

For the optical communication, there exist the coherent and the non-coherent communication schemes. With the coherent scheme, both the intensity and the phase of the optical carrier carry information. However, the system architecture is complicated and the related optical devices are expensive. The scheme is usually used in the optical fiber communication system [3]. With the non-coherent scheme, only the intensity of the optical carrier carries information, which is named as the intensity modulation (IM) and adopted in the OWC system

[2], [4]. The intensity of the optical carrier is real and non-negative, hence also the modulated RF signal.

The orthogonal frequency division multiplexing (OFDM) waveform is a key feature in the 4G and the 5G RF communication [5], which is also utilized in IEEE 802.15.13, IEEE 802.11b and ITU-9991 standards for the OWC [6]–[8]. To satisfy the real and non-negative requirements, the OFDM waveform is modified as the DC-biased optical OFDM (DCO-OFDM) waveform, the unipolar OFDM (U-OFDM) waveform and the asymmetrically clipped optical OFDM (ACO-OFDM) waveform. The Hermitian symmetry (HS) character of the signal in the frequency domain, guarantees the signal in the time domain to be real at the sacrifice of $1/2$ spectral efficiency. To be non-negative, the DCO-OFDM waveform adds the DC bias and clips the negative parts with $1/2$ spectral efficiency. Without the DC bias, the U-OFDM waveform flips the negative parts following the non-negative parts, which doubles the signal length in the time domain with $1/4$ spectral efficiency. The ACO-OFDM waveform only uses the odd sub-carriers in the frequency domain with $1/4$ spectral efficiency. Then the signal in the time domain is antisymmetric, and the negative parts are clipped directly [9].

To further increase the spectral efficiency and reduce the power consumption, the hybrid approach as the asymmetrically clipped DC biased optical OFDM (ADO-OFDM) waveform [10] and the superposition approach as the layered ACO-OFDM waveform [11] and the enhanced U-OFDM waveform [12] are analyzed. The ADO-OFDM waveform combines the DCO-OFDM at the even sub-carriers and the ACO-OFDM at the odd sub-carriers. The layered ACO-OFDM waveform has multiple layers, where each layer uses the carefully selected sub-carriers. The enhanced U-OFDM waveform has multiple depths, where each depth repeats the signal multiple times. However, all the receivers require the successive demodulation scheme, where part of the signal is demodulated and reconstructed to erase the interference, before other parts of the signal to be demodulated. The receiver is complicated and suffers from the error propagation problem [13].

In this paper, two types of mixed OFDM (X-OFDM) waveform without the DC bias are proposed, where the first type of X-OFDM waveform uses the non-successive demodulation scheme. Similarly, for the signal in the time domain to be real, the N sub-carriers in the frequency domain satisfy the HS requirement. Then the sub-carriers are divided into the odd sub-carriers and the even sub-carriers. For the odd sub-carriers, after the inverse fast fourier transform (IFFT), the

X. Li, J. Huang, Y. Lyu, R. Ni, J. Luo, J. Zhang are with the Shenzhen Research Development Center, Huawei Technologies Co., Ltd., 518129, China.

Corresponding author: X. Li, e-mail: lixu11@huawei.com.

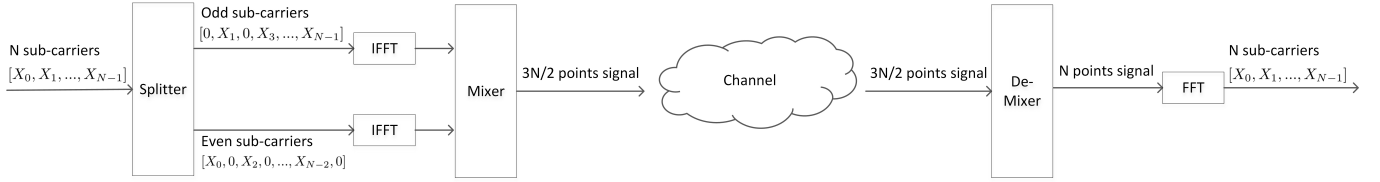


Fig. 1. The system architecture of the first type of X-OFDM waveform.

signal in time domain is antisymmetric, where the first $N/2$ points are the inverse of the second $N/2$ points. For the even sub-carriers, after the IFFT, the signal in the time domain is symmetric, where the first $N/2$ points equal to the second $N/2$ points. Then there are four independent $N/2$ points extracted as: 1) the non-negative parts of the first $N/2$ points generated from the odd sub-carriers; 2) the negative parts of the first $N/2$ points generated from the odd sub-carriers; 3) the non-negative parts of the first $N/2$ points generated from the even sub-carriers; 4) the negative parts of the first $N/2$ points generated from the even sub-carriers. The four independent $N/2$ points are mixed to be a $3N/2$ points sequence at the transmitter and de-mixed to be decoded at the receiver in different ways for the two types of X-OFDM waveform. The spectral efficiency, computational complexity, motivation and comparison are discussed, and the numerical simulations are provided to evaluate the performance of the two types of X-OFDM waveform.

The first type of X-OFDM waveform is briefly introduced in our conference paper [14], but comprehensively studied along with the second type of X-OFDM waveform in this paper. The contributions of this paper are summarized as:

- Two types of X-OFDM waveform without the DC bias are proposed for the OWC with the IM, where the modulated RF signal is real and non-negative;
- The related system architecture, signal processing, spectrum efficiency, computational complexity, motivation and comparison, and numerical simulations considering the relative intensity noise, shot noise, background radiation noise and thermal noise of the OWC channel [15] are comprehensively studied;
- The first type of X-OFDM waveform uses the non-successive demodulation scheme, which has $1/3$ spectral efficiency, $\mathcal{O}(3N \log_2 N)$ computational complexity, low peak to average power ratio (PAPR) and high power efficiency especially for the scenarios with the high relative intensity noise and shot noise;
- The second type of X-OFDM waveform uses the successive demodulation scheme, which has $1/3$ spectral efficiency, $\mathcal{O}(5N \log_2 N)$ computational complexity, higher PAPR but higher power efficiency than the first type of X-OFDM waveform especially for the scenarios with the high relative intensity noise and shot noise.

The remainder of this paper is organized as follows. Section II introduces the first type of X-OFDM waveform with the system architecture and the signal processing at the transmitter and the receiver. Section III introduces the second type of X-OFDM waveform with the system architecture and the

signal processing at the transmitter and the receiver. The spectral efficiency, computational complexity, motivation and comparison are discussed in Section IV. Section V presents the numerical simulations, followed by the conclusions in Section VI.

II. THE FIRST TYPE OF X-OFDM WAVEFORM

The first type of X-OFDM waveform guarantees the signal in the time domain to be real and non-negative, without the DC bias and with the non-successive demodulation scheme. This section studies the system architecture and the signal processing at the transmitter and the receiver of the first type of X-OFDM waveform.

A. System Architecture

The system architecture of the first type of X-OFDM waveform is shown in Fig. 1. At the transmitter, there exist a splitter, two IFFT blocks, and a mixer. The splitter splits the N sub-carriers into the odd sub-carriers and the even sub-carriers. The IFFT blocks transform the signal into the time domain, followed by the mixer to generate a $3N/2$ points signal. At the receiver, there exist a de-mixer and a FFT block. Based on the $3N/2$ points signal, the de-mixer constructs a N points signal, followed by the FFT block to recover the N sub-carriers.

B. Signal Processing at Transmitter

The OWC with the IM, requires the modulated RF signal to be real and non-negative. To be real, the HS character of the sub-carriers in the frequency domain $[X_0, X_1, \dots, X_{N-1}]$ is used as [9]:

$$\begin{aligned} X_m &= X_{N-m}^*, 0 < m < \frac{N}{2}. \\ X_0 &= X_{\frac{N}{2}} = 0 \end{aligned} \quad (1)$$

and the signal in the time domain is:

$$\begin{aligned} x_k^{origin} &= \sum_{m=0}^N X_m \exp\left(j \frac{2\pi}{N} mk\right) \\ &= \text{Real} \left\{ 2 \sum_{m=0}^{\frac{N}{2}} X_m \exp\left(j \frac{2\pi}{N} mk\right) \right\} \end{aligned} \quad (2)$$

which is shown in Fig.2a. The first $N/2$ points are defined as L , and the second $N/2$ points are defined as R , where both L and R are real. We note that the IFFT equation (2) and Fig.2a are shown for easier understanding of the X-OFDM waveform, but not needed in the real system.

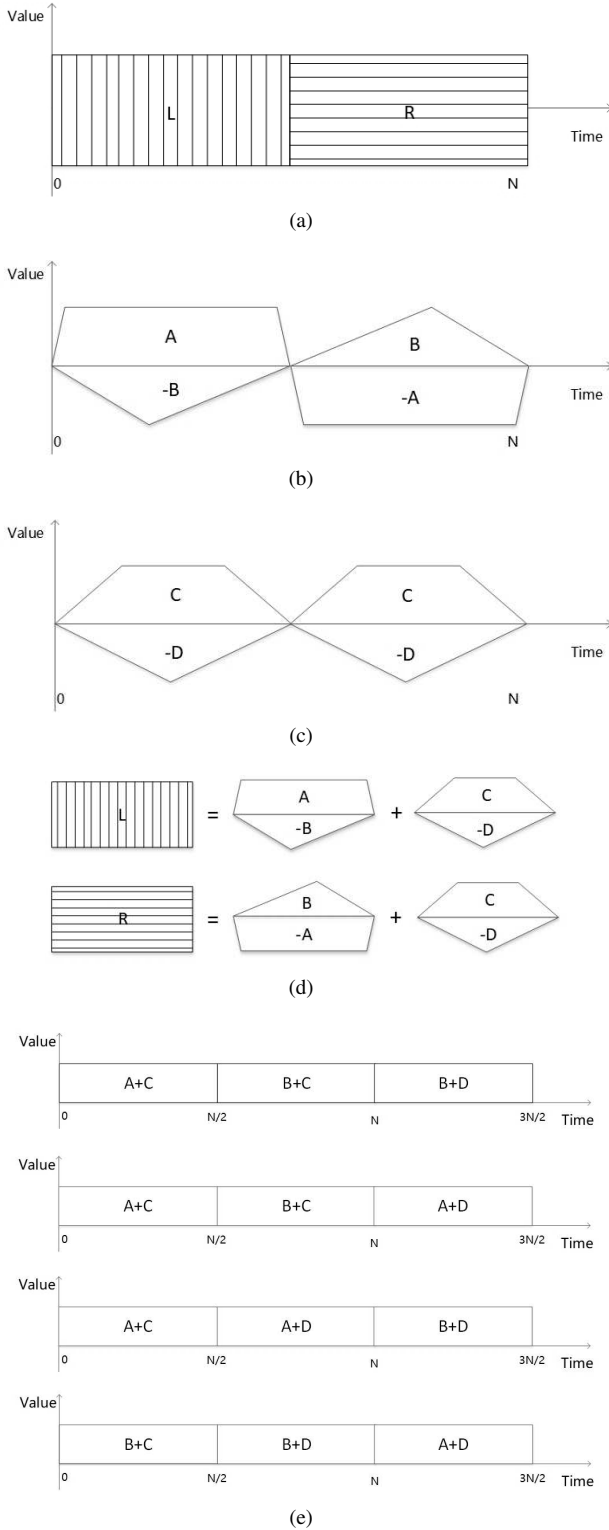


Fig. 2. The signal processing at the transmitter of the first type of the X-OFDM waveform: (a) the real signal in the time domain with the sub-carriers satisfying the HS requirement, (b) the antisymmetric signal in the time domain with the odd sub-carriers, (c) the symmetric signal in the time domain with the even sub-carriers, (d) the relationship of the signal in the time domain, (e) the candidate transmitted signal in the time domain.

The splitter splits the N sub-carriers into the odd sub-carriers as $[0, X_1, 0, X_3, \dots, X_{N-1}]$ and the even sub-carriers as $[X_0, 0, X_2, 0, \dots, X_{N-2}, 0]$. For the odd sub-carriers, after the IFFT block, the signal in the time domain satisfies:

$$\begin{aligned} x_{k+\frac{N}{2}}^{odd} &= \sum_{m=0}^{\frac{N}{2}-1} X_{2m+1} \exp\left(j\frac{2\pi}{N}(2m+1)\left(k+\frac{N}{2}\right)\right) \\ &= \sum_{m=0}^{\frac{N}{2}-1} X_{2m+1} \exp\left(j\frac{2\pi}{N}(2m+1)k\right) \exp(j\pi(2m+1)) \\ &= -x_k^{odd} \end{aligned} \quad (3)$$

which is antisymmetric as shown in Fig.2b. For the first $N/2$ points, the non-negative parts are defined as A , and the negative parts are defined as $-B$, where both $A = [x_0^A, x_1^A, \dots, x_{\frac{N}{2}-1}^A]$ and $B = [x_0^B, x_1^B, \dots, x_{\frac{N}{2}-1}^B]$ are real and non-negative as:

$$x_k^A = \frac{|x_k^{odd}| + x_k^{odd}}{2}, 0 \leq k < \frac{N}{2} \quad (4)$$

$$x_k^B = \frac{|x_k^{odd}| - x_k^{odd}}{2}, 0 \leq k < \frac{N}{2} \quad (5)$$

For the even sub-carriers, after the IFFT block, the signal in the time domain satisfies:

$$\begin{aligned} x_{k+\frac{N}{2}}^{even} &= \sum_{m=0}^{\frac{N}{2}-1} X_{2m} \exp\left(j\frac{2\pi}{N}(2m)\left(k+\frac{N}{2}\right)\right) \\ &= \sum_{m=0}^{\frac{N}{2}-1} X_{2m+1} \exp\left(j\frac{2\pi}{N}(2m)k\right) \exp(j\pi(2m)) \\ &= x_k^{even} \end{aligned} \quad (6)$$

which is symmetric as shown in Fig.2c. For the first $N/2$ points, the non-negative parts are defined as C , and the negative parts are defined as $-D$, where both $C = [x_0^C, x_1^C, \dots, x_{\frac{N}{2}-1}^C]$ and $D = [x_0^D, x_1^D, \dots, x_{\frac{N}{2}-1}^D]$ are real and non-negative as:

$$x_k^C = \frac{|x_k^{even}| + x_k^{even}}{2}, 0 \leq k < \frac{N}{2} \quad (7)$$

$$x_k^D = \frac{|x_k^{even}| - x_k^{even}}{2}, 0 \leq k < \frac{N}{2} \quad (8)$$

Then there exist the relationships as shown in Fig.2d that:

$$\begin{aligned} L &= (A + C) - (B + D) \\ R &= (B + C) - (A + D) \end{aligned} \quad (9)$$

and

$$(A + C) + (B + D) = (B + C) + (A + D). \quad (10)$$

Based on the relationships, we could transmit either three of $(A + C)$, $(B + D)$, $(B + C)$, $(A + D)$ as shown in Fig.2e, and recover the remaining one using equation (10). The function of the mixer block is summarized as:

- The A , B , C , D are extracted using the equations (4), (5), (7) and (8);
- The A , B , C , D are mixed to construct either three of $(A + C)$, $(B + D)$, $(B + C)$, $(A + D)$ as shown in Fig.2e.

Then the constructed $3N/2$ points are transmitted at the transmitter.

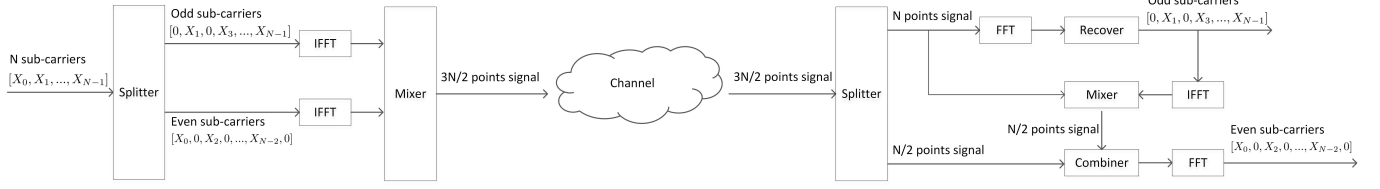


Fig. 3. The system architecture of the second type of X-OFDM waveform.

C. Signal Processing at Receiver

The receiver receives the $3N/2$ points of either three of $(A + C)$, $(B + D)$, $(B + C)$, $(A + D)$ as shown in Fig.2e. Based on the received signal, the de-mixer constructs the N points signal as shown in Fig.2a as:

- The remaining one of $(A + C)$, $(B + D)$, $(B + C)$, $(A + D)$ is recovered using equation (10);
- The L and R are constructed using equation (9).

The N points signal as shown in Fig.2a goes through the FFT block to recover the N sub-carriers in the frequency domain as $[X_0, X_1, \dots, X_{N-1}]$.

D. An Example

A simple example is provided for the first type of X-OFDM waveform. At the transmitter, the sub-carrier number is $N = 8$ and the constellation is 16-QAM. The signal of the sub-carriers are:

N = 8 sub-carriers $[X_0, X_1, \dots, X_7]$ satisfying the HS requirement							
0	-3-j	-3+j	-1+3j	0	-1-3j	-3-j	-3+j

The odd sub-carriers and A, B are:

The odd sub-carriers $[0, X_1, 0, X_3, \dots, 0, X_7]$							
0	-3-j	0	-1+3j	0	-1-3j	0	-3+j
After the IFFT block to get $[x_0^{odd}, x_1^{odd}, \dots, x_7^{odd}]$							
-1	-0.71	1	0	1	0.71	-1	0
A				B			
0	0	1	0	1	0.71	0	0

The even sub-carriers and C, D are:

The even sub-carriers $[X_0, 0, X_2, 0, \dots, X_6, 0]$							
0	0	-3+j	0	0	0	-3-j	0
After the IFFT block to get $[x_0^{even}, x_1^{even}, \dots, x_7^{even}]$							
-0.75	-0.25	0.75	0.25	-0.75	-0.25	0.75	0.25
C				D			
0	0	0.75	0.25	0.75	0.25	0	0

Using the first candidate $3N/2$ points shown in Fig.2e, the transmitted signal is:

$(A + C)$				$(B + C)$				$(B + D)$			
0	0	1.75	0.25	1	0.71	0.75	0.25	1.75	0.96	0	0

At the receiver, $(A + D)$ is recovered as:

$(A + D) = (A + C) + (B + D) - (B + C)$			
0.75	0.25	1	0

Then L and R shown in Fig.2a are constructed, followed by the FFT block to recover the N sub-carriers as:

$L = (A + C) - (B + D)$				$R = (B + C) - (A + D)$			
-1.75	-0.96	1.75	0.25	0.25	0.46	-0.25	0.25
After the FFT block to recover $[X_0, X_1, \dots, X_7]$							
0	-3-j	-3+j	-1+3j	0	-1-3j	-3-j	-3+j

It could be seen that the messages carried by all sub-carriers are recovered.

III. THE SECOND TYPE OF X-OFDM WAVEFORM

The second type of X-OFDM waveform is proposed to further increase the spectral efficiency at the sacrifice of the computational complexity, which are discussed in Section IV. This section studies the system architecture and the signal processing at the transmitter and the receiver of the second type of X-OFDM waveform.

A. System Architecture

The system architecture of the second type of X-OFDM waveform is shown in Fig. 3. At the transmitter, there exist a splitter, two IFFT blocks, and a mixer. The splitter splits the N sub-carriers into the odd sub-carriers and the even sub-carriers. The IFFT blocks transform the signal into the time domain, followed by the mixer to generate a $3N/2$ points signal. We note that the mixer is different to that of the first type of X-OFDM waveform. At the receiver, there exist a splitter, a recover, a mixer, a combiner, a IFFT and two FFT blocks. The splitter splits the $3N/2$ points into a N points signal and a $N/2$ points signal. The FFT and recover blocks recover the odd sub-carriers. Then the mixer, combiner, IFFT and FFT blocks utilize the odd sub-carriers to successively recover the even sub-carriers.

B. Signal Processing at Transmitter

Similarly, the HS character of the sub-carriers in the frequency domain $[X_0, X_1, \dots, X_{N-1}]$ guarantees the signal in the time domain to be real. The splitter splits the N sub-carriers into the odd sub-carriers as $[0, X_1, 0, X_3, \dots, X_{N-1}]$ and the even sub-carriers as $[X_0, 0, X_2, 0, \dots, X_{N-2}, 0]$. After the two IFFT blocks, the signal in the time domain is obtained as Fig.2b and Fig.2c.

Then we could transmit either $(A + C)$, $(B + C)$, D or $(A + D)$, $(B + D)$, C as shown in Fig. 4. The function of the mixer block is summarized as:

- The A, B, C, D are extracted using the equations (4), (5), (7) and (8);
- The A, B, C, D are mixed to construct either $(A + C)$, $(B + C)$, D or $(A + D)$, $(B + D)$, C as shown in Fig.4.

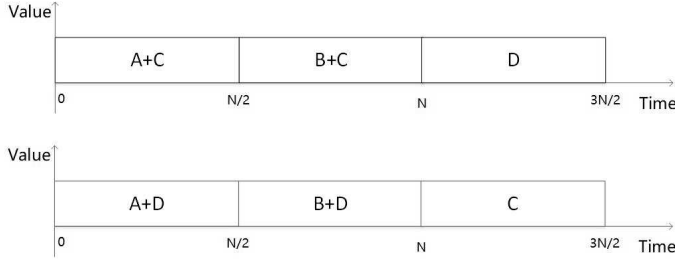


Fig. 4. The candidate transmitted signal in the time domain of the second type of X-OFDM waveform.

Then the constructed $3N/2$ points are transmitted at the transmitter.

C. Signal Processing at Receiver

The receiver receives the $3N/2$ points of either $(A + C)$, $(B + C)$, D or $(A + D)$, $(B + D)$, C as shown in Fig.4. In the following, the $3N/2$ points $(A + C)$, $(B + C)$, D are analyzed to recover the sub-carriers, and the $3N/2$ points $(A + D)$, $(B + D)$, C follow the same way and are omitted to save space.

The splitter splits the $3N/2$ points $(A + C)$, $(B + C)$, D into the N points $(A + C)$, $(B + C)$ and the $N/2$ points D . Based on the N points $(A + C)$, $(B + C)$, the odd sub-carriers are recovered by the FFT and recover blocks. Assuming the signal after the FFT block is $[Y_0, Y_1, \dots, Y_{N-1}]$, we have:

$$Y_{2m+1} = \sum_{k=0}^{\frac{N}{2}-1} (x_k^A + x_k^C) \exp\left(-j\frac{2\pi}{N}(2m+1)k\right) + \sum_{k=0}^{\frac{N}{2}-1} (x_k^B + x_k^C) \exp\left(-j\frac{2\pi}{N}(2m+1)\left(k + \frac{N}{2}\right)\right) \quad (11a)$$

$$= \sum_{k=0}^{\frac{N}{2}-1} ((x_k^A + x_k^C) - (x_k^B + x_k^C)) \exp\left(-j\frac{2\pi}{N}(2m+1)k\right) \quad (11b)$$

$$= \sum_{k=0}^{\frac{N}{2}-1} (x_k^A - x_k^B) \exp\left(-j\frac{2\pi}{N}(2m+1)k\right) \quad (11c)$$

$$= \frac{1}{2} \left(\sum_{k=0}^{\frac{N}{2}-1} (x_k^A - x_k^B) \exp\left(-j\frac{2\pi}{N}(2m+1)k\right) + \sum_{k=\frac{N}{2}}^{N-1} (x_k^B - x_k^A) \exp\left(-j\frac{2\pi}{N}(2m+1)k\right) \right) \quad (11d)$$

$$= \frac{X_{2m+1}}{2}, 0 \leq m < \frac{N}{2} \quad (11e)$$

where equation (11a) uses the N points $(A + C)$, $(B + C)$ and equation (11d) to equation (11e) utilizes Fig. 2b and the inverse of equations (3), (4) and (5). The recover block selects the odd parts multiplying by two to recover the odd sub-carriers $[0, X_1, 0, X_3, \dots, X_{N-1}]$.

Then the even sub-carriers $[X_0, 0, X_2, 0, \dots, X_{N-2}, 0]$ are recovered by the IFFT, mixer, combiner and FFT blocks. The IFFT block transforms the odd sub-carriers to the signal in the time domain as shown in Fig.2b. The function of the mixer block is summarized as:

- The A , B are extracted using equations (4), (5);
- The A , B and $(A + C)$, $(B + C)$ are mixed to obtain C .

The $N/2$ points C could be obtained by $(A + C) - A$, $(B + C) - B$ or $\frac{(A+C)-A+(B+C)-B}{2}$, where the third one uses the average to reduce the noise. Based on the $N/2$ points C from the mixer block and the $N/2$ points D from the splitter block, the combiner block constructs $(C - D)$, $(C + D)$ as shown in Fig.2c. The FFT block transforms the signal in the time domain to recover the odd sub-carriers as $[X_0, 0, X_2, 0, \dots, X_{N-2}, 0]$.

D. An Example

Similarly, a simple example is provided for the second type of X-OFDM waveform. At the transmitter, the sub-carrier number is $N = 8$ and the constellation is 16-QAM. The signal of the sub-carriers are:

N = 8 sub-carriers $[X_0, X_1, \dots, X_7]$ satisfying the HS requirement							
0	-3-j	-3+j	-1+3j	0	-1-3j	-3-j	-3+j

The odd sub-carriers and A , B are:

The odd sub-carriers $[0, X_1, 0, X_3, \dots, 0, X_7]$							
0	-3-j	0	-1+3j	0	-1-3j	0	-3+j
After the IFFT block to get $[x_0^{odd}, x_1^{odd}, \dots, x_7^{odd}]$							
-1	-0.71	1	0	1	0.71	-1	0
A				B			
0	0	1	0	1	0.71	0	0

The even sub-carriers and C , D are:

The even sub-carriers $[X_0, 0, X_2, 0, \dots, X_6, 0]$							
0	0	-3+j	0	0	0	-3-j	0
After the IFFT block to get $[x_0^{even}, x_1^{even}, \dots, x_7^{even}]$							
-0.75	-0.25	0.75	0.25	-0.75	-0.25	0.75	0.25
C				D			
0	0	0.75	0.25	0.75	0.25	0	0

Using the first candidate $3N/2$ points shown in Fig.4, the transmitted signal is:

(A + C)				(B + C)				D			
0	0	1.75	0.25	1	0.71	0.75	0.25	0.75	0.25	0	0

At the receiver, the input signal is split as:

(A + C)				(B + C)			
0	0	1.75	0.25	1	0.71	0.75	0.25

D			
0.75	0.25	0	0

The odd sub-carriers are recovered as:

(A + C)				(B + C)			
0	0	1.75	0.25	1	0.71	0.75	0.25
After the FFT block to get $[Y_0, Y_1, \dots, Y_7]$							
4.71	-1.5	-1.5	-0.5	2.29	-0.5	-1.5	-1.5
	-0.5j	-0.2j	+1.5j		-1.5j	+0.2j	+0.5j
After the recover block to get $[0, X_1, 0, X_3, \dots, 0, X_7] = 2 \times [0, Y_1, 0, Y_3, \dots, 0, Y_7]$							
0	-3-j	0	-1+3j	0	-1-3j	0	-3+j

The even sub-carriers are recovered by four steps. The first step re-extracts A , B as:

Odd sub-carriers $[0, X_1, 0, X_3, \dots, 0, X_7]$							
0	-3-j	0	-1+3j	0	-1-3j	0	-3+j
After IFFT to get $[x_0^{odd}, x_1^{odd}, \dots, x_7^{odd}]$							
-1	-0.71	1	0	1	0.71	-1	0
A				B			
0	0	1	0	1	0.71	0	0

The second step re-constructs C as:

$$C = (A+C) - A = (B+C) - B = \frac{(A+C) - A + (B+C) - B}{2}$$

0	0	0.75	0.25
---	---	------	------

The third step combines C , D as:

(C - D)				(C - D)			
-0.75	-0.25	0.75	0.25	-0.75	-0.25	0.75	0.25

The fourth step recovers the even sub-carriers as:

After the FFT block to recover $[X_0, 0, X_2, 0, \dots, X_6, 0]$							
0	0	-3+j	0	0	0	-3-j	0

It could be seen that the messages carried by the odd sub-carriers and the even sub-carriers are recovered successively.

IV. DISCUSSIONS

The spectral efficiency, computational complexity, motivation and comparison of the proposed two types of X-OFDM waveform are discussed in this section.

A. Spectral Efficiency

Due to the HS requirement, the second half sub-carriers is determined by the first half sub-carriers as equation (1), at the sacrifice of 1/2 spectral efficiency. In the time domain, the transmitted signal extends the N sub-carriers to $3N/2$ points as shown in Fig. 2e and Fig. 4, at the sacrifice of 2/3 spectral efficiency. Hence the spectral efficiency for the two types of X-OFDM waveform is:

$$SE = 1/3 = 1/2 \times 2/3. \quad (12)$$

Moreover, the spectral efficiency is 1/2 for the DCO-OFDM waveform, and 1/4 for the ACO-OFDM waveform and the U-OFDM waveform [9], [10].

B. Complexity

The computational complexity is defined as the number of the multiplications and the additional operations at both the transmitter and the receiver. For an IFFT/FFT block with size of N , it requires approximately $N \log(N)$ operations [16],

[17]. For the system architecture of the first type of X-OFDM waveform shown in Fig. 1, it has two IFFT blocks at the transmitter and one FFT block at the receiver. The computational complexity is around $3N \log(N)$. For the system architecture of the second type of X-OFDM waveform shown in Fig. 3, it has two IFFT blocks at the transmitter and two FFT and one IFFT blocks at the receiver. The computational complexity is around $5N \log(N)$. Then the total computational complexity of the DCO-OFDM, the ACO-OFDM, the U-OFDM and the two types of X-OFDM waveform are summarized in TABLE I.

TABLE I
THE COMPUTATIONAL COMPLEXITY OF THE DCO-OFDM, THE ACO-OFDM, THE U-OFDM AND THE TWO TYPES OF X-OFDM WAVEFORM.

OFDM Waveforms	Number of IFFT block at transmitter	Number of FFT/IFFT block at receiver	Total computational complexity
DCO-OFDM	1	1	$\mathcal{O}(2N \log_2 N)$
ACO-OFDM	1	1	$\mathcal{O}(2N \log_2 N)$
U-OFDM	1	1	$\mathcal{O}(2N \log_2 N)$
First type of X-OFDM	2	1	$\mathcal{O}(3N \log_2 N)$
Second type of X-OFDM	2	3	$\mathcal{O}(5N \log_2 N)$

C. Motivation and Comparison

The proposed two types of X-OFDM waveform utilize the antisymmetric and symmetric characters of the signal in the time domain, when the odd and even sub-carriers in the frequency domain satisfy the HS requirement.

For the first type of X-OFDM waveform, based on the forward analysis with the IFFT block, the key motivation is the relationship as equation (10). Then either three of $(A+C)$, $(B+D)$, $(B+C)$, $(A+D)$ as shown in Fig.2e are transmitted, and the remaining one is recoverable. However, the recovering operation highly increase the noise. For an example with $(A+C)$, $(B+D)$, $(B+C)$ being transmitted, and the thermal noise with variance σ^2 at the receiver, we re-write equation (9) as:

$$\begin{aligned} L &= (A + C) - (B + D) \\ R &= 2(B + C) - (A + C) - (B + D) \end{aligned} \quad (13)$$

The add and subtract operations increase the noise variance of L and R to be $2\sigma^2$ and $6\sigma^2$, which degrade the system data rate even that the noise of L and R are dependent.

For the second type of X-OFDM waveform, to decrease the influence of noise and based on the backward analysis with the FFT block, the key motivation is as follows:

- For the even sub-carriers satisfying the HS requirement, after the IFFT block, the signal in the time domain is symmetric as shown in Fig.2c.
- Reversely, for the symmetric signal in the time domain, after the FFT block, the signal has values at the even sub-carriers, but equals 0 at the odd sub-carriers.
- Then for the N points signal $(A + C)$, $(B + C)$ or $(A + D)$, $(B + D)$ in the time domain, after the FFT block,

the signal has useless values at the even sub-carriers, but recovers the odd sub-carriers.

- Once the odd sub-carriers are recovered, the even sub-carriers could be recovered successively.

The procedures of the second type of X-OFDM waveform are complicated, but do not have the add and subtract operations, which could decrease the noise and enhance the system data rate.

Therefore, the first type X-OFDM waveform has the lower system data rate, but the lower computational complexity. The second type X-OFDM waveform has the higher system data rate, but the higher computational complexity.

V. NUMERICAL SIMULATIONS

In this section, numerical simulations are provided to evaluate the performance of the proposed two types of X-OFDM waveform.

A. Definitions

For the simulations, we consider the improved free-space optical intensity channel [15], [18], [19] as:

$$Y = X + \sqrt{X}Z_1 + Z_0 \quad (14)$$

where X is the received signal generated by the DCO-OFDM, the ACO-OFDM, the U-OFDM, or the two types of X-OFDM waveform, Z_0 is the signal-independent Gaussian noise with zero mean and σ^2 variance, and Z_1 is the signal-dependent Gaussian noise with zero mean and ξ^2 variance. The signal-independent noise mainly consists of the background radiation noise received by the photodiode (PD) and the thermal noise from the electrical circuits at the receiver [20], [21]. The signal-dependent noise mainly has the relative intensity noise from the laser diode (LD) or light emitting diode (LED) [22], [23] at the transmitter and the shot noise from the PD [24], [25] at the receiver.

The electrical power per bit to the signal-dependent noise ratio is defined as:

$$\langle E_{b(elec)}/\xi^2 \rangle = \frac{E(X^2)}{\xi^2 \cdot b_s} \quad (15)$$

where b_s is the number of bits per symbol depending on the constellation and the spectral efficiency.

The electrical power per bit to signal-independent noise ratio is defined as:

$$\langle E_{b(elec)}/\sigma^2 \rangle = \frac{E(X^2)}{\sigma^2 \cdot b_s} \quad (16)$$

Regardless of the electrical current threshold, the output optical power of the LD or LED increases linearly with the input electrical current [22], [23]. Hence the optical power per bit to signal-dependent noise ratio is defined as:

$$\langle E_{b(opt)}/\xi^2 \rangle = \frac{E(X)}{\xi^2 \cdot b_s} \quad (17)$$

The optical power per bit to signal-independent noise ratio is defined as:

$$\langle E_{b(opt)}/\sigma^2 \rangle = \frac{E(X)}{\sigma^2 \cdot b_s} \quad (18)$$

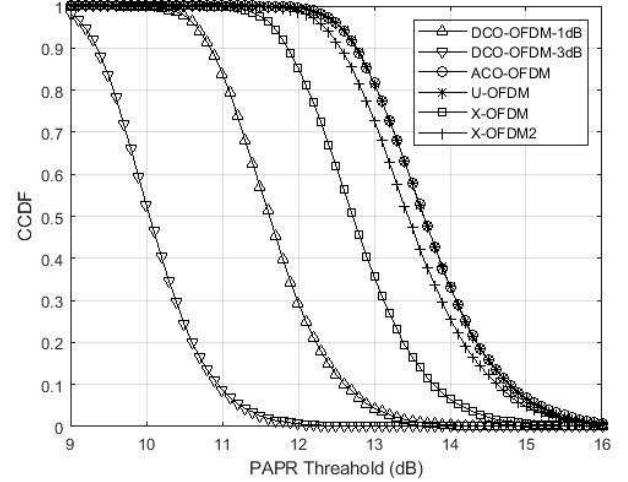


Fig. 5. The CCDF of the PAPR for the DCO-OFDM with 1dB and 3dB DC bias level, the ACO-OFDM, the U-OFDM and the two types of X-OFDM waveform.

For the DCO-OFDM waveform, the DC bias level is set relative to the standard deviation of X . With the DC bias as:

$$DC_{bias} = \mu\sqrt{E(X^2)}, \quad (19)$$

the bias level is $10 \log_{10}(\mu^2 + 1)$ dB [10].

B. Simulations

Using Monte Carlo simulation, the results are the average of 2000 OFDM symbols with 2048 sub-carriers, for different constellation, waveform, bit error rate (BER), $\langle E_{b(elec)}/\xi^2 \rangle$, $\langle E_{b(opt)}/\xi^2 \rangle$, $\langle E_{b(elec)}/\sigma^2 \rangle$, and $\langle E_{b(opt)}/\sigma^2 \rangle$.

1) *PAPR Performance*: The complementary cumulative distribution function (CCDF) of the PAPR for the DCO-OFDM with 1dB and 3dB DC bias level, the ACO-OFDM, the U-OFDM and the two types of X-OFDM waveform are shown in Fig. 5. It could be seen that the PAPR performance of the ACO-OFDM waveform and that of the U-OFDM waveform overlap each other. The DCO-OFDM waveform with the DC bias outperforms the ACO-OFDM/U-OFDM and the two types of X-OFDM waveform without the DC bias. Meanwhile, the PAPR performance gets better as the DC bias level of the DCO-OFDM waveform increases. The reason is that, for the DCO-OFDM waveform, both the peak power and the average power increase with the DC bias level. For the scenarios without the DC bias, the first type of X-OFDM waveform has the best PAPR performance. The second type of X-OFDM waveform has better PAPR performance than that of the ACO-OFDM/U-OFDM waveform.

2) *BER Performance*: The BER performance of the two types of X-OFDM waveform are provided for the scenario with only the signal-dependent noise, and the other scenarios are compared in next subsection.

For the two types of X-OFDM, when only the signal-independent noise exists, the BER against the $\langle E_{b(elec)}/\xi^2 \rangle$ and the $\langle E_{b(opt)}/\xi^2 \rangle$ are shown in Fig.6 and Fig.7. It is observed that the second type of X-OFDM waveform has

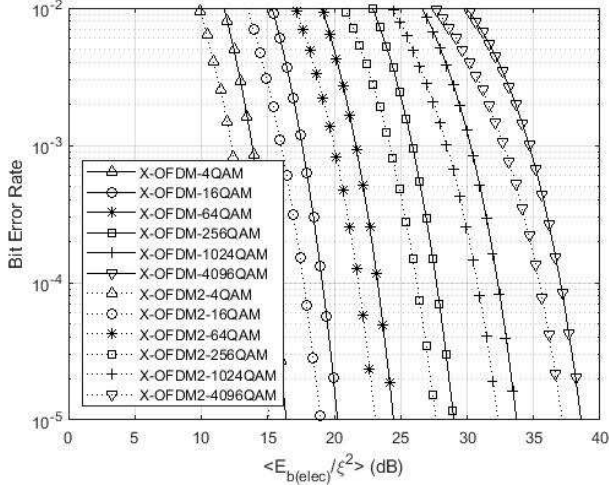


Fig. 6. The BER against the $\langle E_{b(elec)}/\xi^2 \rangle$ for the two types of X-OFDM waveform, when only the signal-dependent noise exists.

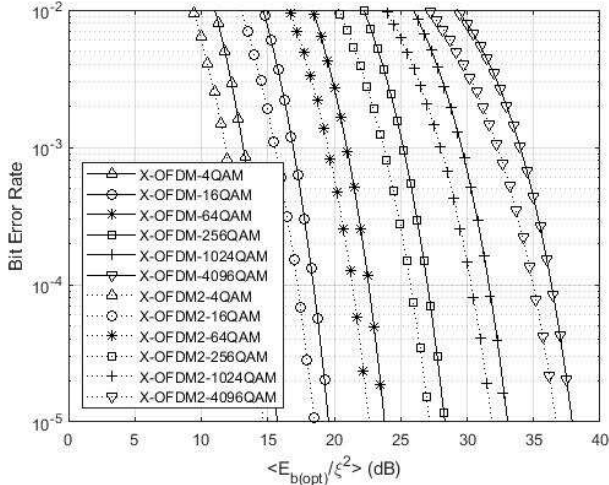


Fig. 7. The BER against the $\langle E_{b(opt)}/\xi^2 \rangle$ for the two types of X-OFDM waveform, when only the signal-dependent noise exists.

better BER performance with the same $\langle E_{b(elec)}/\xi^2 \rangle$ or $\langle E_{b(opt)}/\xi^2 \rangle$. Since the decoding is processed in the electrical domain, the analysis in Section IV-C explains the reason that the second type of X-OFDM waveform has better BER performance with the same $\langle E_{b(elec)}/\xi^2 \rangle$. The simulation results show that this character also holds for the $\langle E_{b(opt)}/\xi^2 \rangle$.

3) *Performance Comparison with the BER of 10^{-3}* : The required $\langle E_{b(elec)}/\xi^2 \rangle$, $\langle E_{b(opt)}/\xi^2 \rangle$, $\langle E_{b(elec)}/\sigma^2 \rangle$, and $\langle E_{b(opt)}/\sigma^2 \rangle$ for the BER of 10^{-3} is used for the comparison between the different waveform. During the simulations, the DCO-OFDM waveform with the DC bias level $\{1, 2, 3, 4, 5, 6, 7, 8, 9, 10, 11, 12, 13\}$ dB are simulated, and the optimal ones are selected as the result of the DCO-OFDM waveform with the best DC bias level. Meanwhile, the normalized bit rate of the DCO-OFDM, the ACO-OFDM, the U-OFDM and the two types of X-OFDM waveform are $1/2, 1/4, 1/4$ [9], [10] and $1/3$ spectral efficiency times the

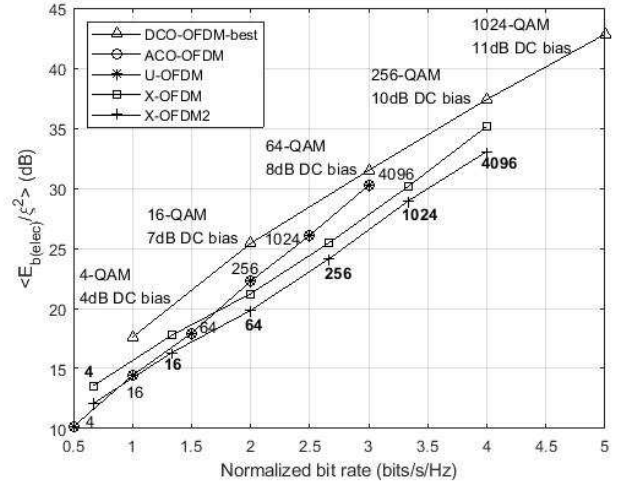


Fig. 8. The $\langle E_{b(elec)}/\xi^2 \rangle$ against the normalized bit rate for the DCO-OFDM with the optimal DC bias level, the ACO-OFDM, the U-OFDM and the two types of X-OFDM waveform, when the BER is 10^{-3} and only the signal-dependent noise exists.

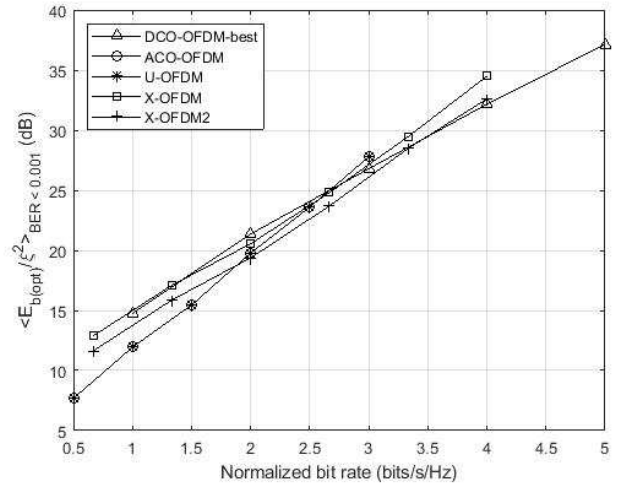


Fig. 9. The $\langle E_{b(opt)}/\xi^2 \rangle$ against the normalized bit rate for the DCO-OFDM with the optimal DC bias level, the ACO-OFDM, the U-OFDM and the two types of X-OFDM waveform, when the BER is 10^{-3} and only the signal-dependent noise exists.

constellation.

For the scenario with only the signal-dependent noise, the best DC bias level for the DCO-OFDM waveform are $\{4, 7, 8, 10, 11\}$ dB for $\{4, 16, 64, 256, 1024\}$ QAM constellation. When the BER is 10^{-3} , the $\langle E_{b(elec)}/\xi^2 \rangle$ and the $\langle E_{b(opt)}/\xi^2 \rangle$ against the normalized bit rate for the different waveform are shown in Fig.8 and Fig.9. It could be seen that the performance of the ACO-OFDM waveform and that of the U-OFDM overlap each other. Meanwhile, the second type of X-OFDM waveform is better than the first type of X-OFDM waveform as discussed before. For the $\langle E_{b(elec)}/\xi^2 \rangle$ in Fig.8, the DCO-OFDM waveform with the best DC bias level has the worst power efficiency. The second type of X-OFDM waveform outperforms the ACO-

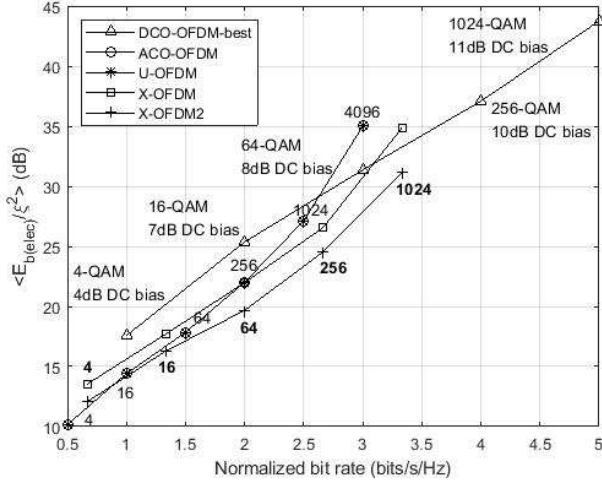


Fig. 10. The $\langle E_{b(elec)}/\xi^2 \rangle$ against the normalized bit rate for the DCO-OFDM with the optimal DC bias level, the ACO-OFDM, the U-OFDM and the two types of X-OFDM waveform, when the BER is 10^{-3} , and the signal-dependent noise exists and the signal-independent noise is set to be $E(X^2)/\sigma^2 = 40$ dB.

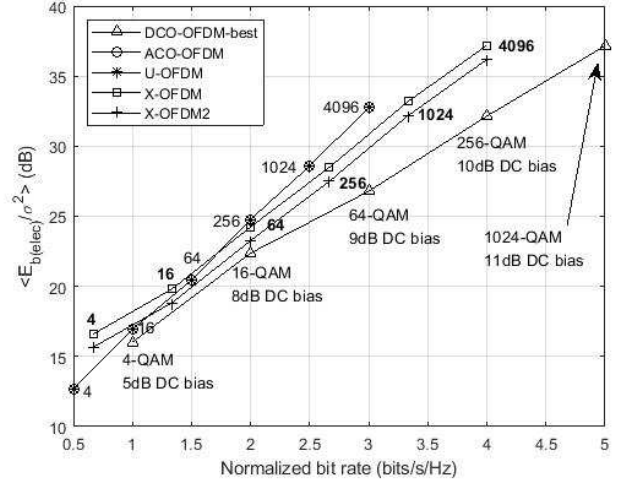


Fig. 12. The $\langle E_{b(elec)}/\sigma^2 \rangle$ against the normalized bit rate for the DCO-OFDM with the optimal DC bias level, the ACO-OFDM, the U-OFDM and the two types of X-OFDM waveform, when the BER is 10^{-3} and only the signal-independent noise exists.

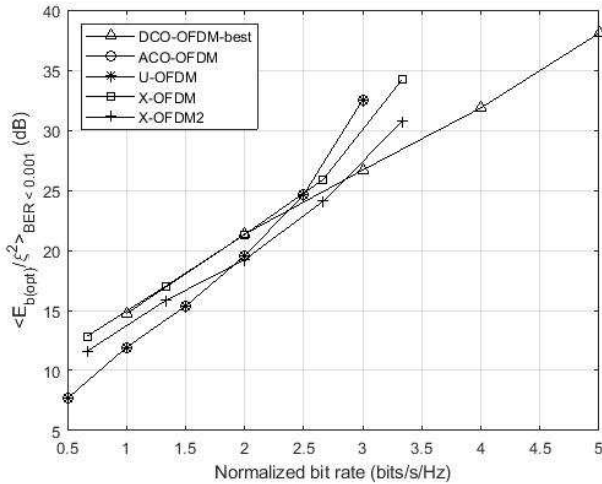


Fig. 11. The $\langle E_{b(opt)}/\xi^2 \rangle$ against the normalized bit rate for the DCO-OFDM with the optimal DC bias level, the ACO-OFDM, the U-OFDM and the two types of X-OFDM waveform, when the BER is 10^{-3} , and the signal-dependent noise exists and the signal-independent noise is set to be $E(X^2)/\sigma^2 = 40$ dB.

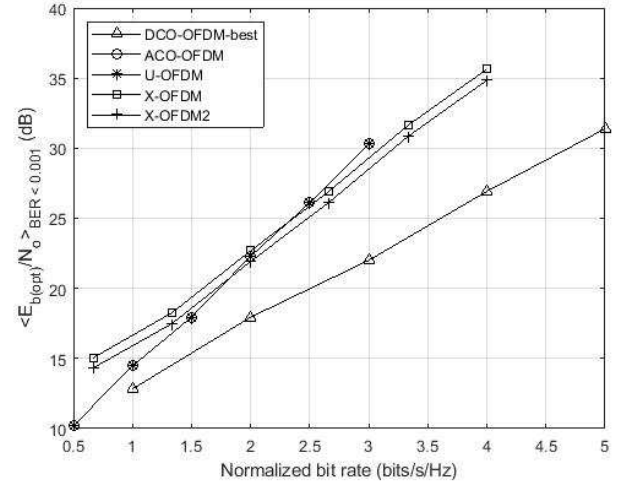


Fig. 13. The $\langle E_{b(opt)}/\sigma^2 \rangle$ against the normalized bit rate for the DCO-OFDM with the optimal DC bias level, the ACO-OFDM, the U-OFDM and the two types of X-OFDM waveform, when the BER is 10^{-3} and only the signal-independent noise exists.

OFDM/U-OFDM waveform and is the best waveform, when the normalized bit rate is larger than 0.9 bits/s/Hz. The first type of X-OFDM waveform outperforms the ACO-OFDM/U-OFDM waveform, when the normalized bit rate is larger than 1.7 bits/s/Hz. For the $\langle E_{b(opt)}/\xi^2 \rangle$ in Fig.9, the best waveform is the ACO-OFDM/U-OFDM waveform, the second type of X-OFDM waveform, and the DCO-OFDM waveform with the best DC bias level, when the normalized bit rate is smaller than 1.88, in [1.88, 3.46], and larger than 3.46 bits/s/Hz respectively.

For the scenario where the signal-dependent noise exists and the signal-independent noise is set to be $\langle E(X^2) \rangle / \sigma^2 = 40$ dB, the best DC bias level are also $\{4, 7, 8, 10, 11\}$ dB for

$\{4, 16, 64, 256, 1024\}$ QAM constellation. When the BER is 10^{-3} , the $\langle E_{b(elec)}/\xi^2 \rangle$ and the $\langle E_{b(opt)}/\xi^2 \rangle$ against the normalized bit rate for the different waveform are shown in Fig.10 and Fig.11. It could be seen that the performance of the ACO-OFDM waveform and that of the U-OFDM waveform overlap each other. Meanwhile, the two types of X-OFDM waveform with the 4096-QAM could not achieve the BER of 10^{-3} with $\langle E(X^2) \rangle / \sigma^2 = 40$ dB, which will be discussed together with the scenario with only the signal-independent noise later. For the $\langle E_{b(elec)}/\xi^2 \rangle$ in Fig.10, the best waveform is the ACO-OFDM/U-OFDM waveform, the second type of X-OFDM waveform, when the normalized bit rate is smaller and larger than 0.9 bit/s/Hz. For the $\langle E_{b(opt)}/\xi^2 \rangle$ in Fig.11, the best waveform is the ACO-OFDM/U-OFDM

waveform, the second type of X-OFDM waveform, and the DCO-OFDM waveform with the best DC bias level, when the normalized bit rate is smaller than 1.91, in [1.91, 2.84], and larger than 2.84 bits/s/Hz respectively.

For the scenario with only the signal-independent noise, the best DC bias level are $\{5, 8, 9, 10, 11\}$ dB for $\{4, 16, 64, 256, 1024\}$ QAM constellation. When the BER is 10^{-3} , the $\langle E_{b(elec)}/\xi^2 \rangle$ and the $\langle E_{b(opt)}/\xi^2 \rangle$ against the normalized bit rate for the different waveform are shown in Fig.12 and Fig.13. It could be seen that the performance of the ACO-OFDM waveform and that of the U-OFDM waveform overlap each other. For the $\langle E_{b(elec)}/\sigma^2 \rangle$ in Fig.12, the DCO-OFDM waveform with the best DC bias level has the best power efficiency. The second and first type of X-OFDM waveform outperforms the ACO-OFDM/U-OFDM waveform, when the normalized bit rate is larger than 1.13 and 1.73 bits/s/Hz. For the $\langle E_{b(opt)}/\sigma^2 \rangle$ in Fig.13, the best waveform is the DCO-OFDM waveform with the best DC bias level. The second and first type of X-OFDM waveform outperforms the ACO-OFDM/U-OFDM waveform, when the normalized bit rate is larger than 1.82 and 2.32 bits/s/Hz.

Moreover, as shown in Fig.12, the required $\langle E_{b(elec)}/\sigma^2 \rangle$ for the two types of X-OFDM waveform with 4096-QAM are 36.2 and 37.2 dB to achieve the BER of 10^{-3} . The normalized bit rate is the bits carried by used sub-carrier $\log_2 4096$ times the spectral efficiency $1/3$, whose value is 4 bits/s/Hz. Referring to the definition of $\langle E_{b(elec)}/\sigma^2 \rangle$ in equation (16), the required $\langle E(X^2)/\sigma^2 \rangle$ for the two types of X-OFDM waveform with 4096-QAM are calculated as 42.2 and 43.2 dB. The simulations in Fig.10 and Fig.11 have $\langle E(X^2)/\sigma^2 \rangle = 40$ dB, which leads to that the 4096-QAM could not achieve the BER of 10^{-3} . We note that $\langle E(X^2)/\sigma^2 \rangle$ is used for the fair comparison with the same channel condition, and $\langle E_{b(elec)}/\xi^2 \rangle$, $\langle E_{b(opt)}/\xi^2 \rangle$, $\langle E_{b(elec)}/\sigma^2 \rangle$ and $\langle E_{b(opt)}/\sigma^2 \rangle$ are utilized for the fair comparison of the power efficiency with the same data rate.

VI. CONCLUSION

In this paper, two types of X-OFDM waveform are proposed for the OWC to satisfy the real and non-negative constrains. The related system architecture, signal processing, spectral efficiency, computational complexity, motivation and comparison, numerical simulations considering the OWC channel are comprehensively studied. Without the DC bias, the proposed two types of X-OFDM waveform achieve $1/3$ spectral efficiency and lower PAPR than the ACO-OFDM/U-OFDM waveform. The first type of X-OFDM waveform uses non-successive demodulation scheme with computational complexity as $\mathcal{O}(3N\log_2(N))$. The second type of X-OFDM waveform uses successive demodulation scheme with computational complexity as $\mathcal{O}(5N\log_2(N))$ and higher power efficiency. With only the signal-dependent noise, the second type of X-OFDM waveform has the best electrical and optical power efficiency, when the normalized bit rate is larger than 0.9 and in [1.88, 3.46] bits/s/Hz, respectively. With only the signal-independent noise and without the DC bias level, the second and first type of X-OFDM waveform outperforms the

ACO-OFDM/U-OFDM waveform, when the normalized bit rate is larger than 1.13 and 1.73 bits/s/Hz for the electrical power efficiency, and 1.82 and 2.32 bits/s/Hz for the optical power efficiency. The proposed two types of X-OFDM waveform could be standardized and utilized in the OWC system in the branch without the DC bias.

REFERENCES

- [1] E. C. Strinati, S. Barbarossa, J. L. Gonzalez-Jimenez, D. Ktenas, N. Cassiau, L. Maret, and C. Dehos, "6G: The Next Frontier: From Holographic Messaging to Artificial Intelligence Using Subterahertz and Visible Light Communication," *IEEE Vehicular Technology Magazine*, vol. 14, no. 3, pp. 42-50, Sep. 2019.
- [2] M. Z. Chowdhury, M. T. Hossan, A. Islam and Y. M. Jang, "A Comparative Survey of Optical Wireless Technologies: Architectures and Applications," *IEEE Access*, vol. 6, pp. 9819-9840, Jan. 2018.
- [3] K. Kikuchi, "Fundamentals of Coherent Optical Fiber Communications," *Journal of Lightwave Technology*, vol. 34, no. 1, pp. 157-179, Jan. 2016.
- [4] L. E. M. Matheus, A. B. Vieira, L. F. M. Vieira, M. A. M. Vieira and O. Gnawali, "Visible Light Communication: Concepts, Applications and Challenges," *IEEE Communications Surveys & Tutorials*, vol. 21, no. 4, pp. 3204-3237, Apr. 2019.
- [5] X. Li, R. Ni, J. Chen, Y. Lyu, Z. Rong and R. Du, "End-to-End Network Slicing in Radio Access Network, Transport Network and Core Network Domains," *IEEE Access*, vol. 8, pp. 29525-29537, Feb. 2020.
- [6] P802.15.13/D6.0 Draft Standard for Multi-Gigabit per Second Optical Wireless Communications (OWC) with Ranges up to 200 Meters, Oct. 2019.
- [7] Draft Text for LC-optimized PHY for TGbb D0.1, Nov. 2019.
- [8] G.9991 High-speed Indoor Visible Light Communication Transceiver System Architecture, Physical Layer and Data Link Layer Specification, Mar. 2019.
- [9] Z. Wang, Q. Wang, W. Huang and Z. Xu, "Visible Light Communications: Modulation and Signal Processing," *Wiley-IEEE Press*, 2018.
- [10] S. D. Dissanayake and Jean Armstrong, "Comparison of ACO-OFDM, DCO-OFDM and ADO-OFDM in IM/DD Systems," *Journal of Lightwave Technology*, vol. 31, no. 7, pp. 1063-1072, Apr. 2013.
- [11] Q. Wang, Z. Wang, X. Guo, and L. Dai, "Improved Receiver Design for Layered ACO-OFDM in Optical Wireless Communications," *IEEE Photonic Technology Letter*, vol. 28, no. 3, pp. 319-322, Feb. 2016.
- [12] D. Tsonev, S. Videv, and H. Haas, "Unlocking Spectral Efficiency in Intensity Modulation and Direct Detection Systems," *IEEE Journal on Selected Areas of Communication*, vol. 33, no. 9, pp. 1758-1770, Sep. 2015.
- [13] A. J. Lowery, "Spectrally Efficient Optical Orthogonal Frequency Division Multiplexing," *Phil. Trans. R. Soc. A.378*, Oct. 2019.
- [14] X. Li, J. Huang, Y. Lyu, J. Luo, J. Zhang, "A Mixed Orthogonal Frequency Division Multiplexing (X-OFDM) Waveform for Optical Wireless Communication," *Accepted by 2020 IEEE GLOBECOM Workshop on Optical Wireless Communications (OWC)*, 2020.
- [15] A.Lapidoth, S.M.Moser, and M.A.Wigger, "On the Capacity of Free-space Optical Intensity Channels," *IEEE Transactions on Information Theory*, vol. 55, no.10, pp.4449-4461, Oct.2009.
- [16] C. Aupetit-Berthelemy and M. F. O. Sanya, "An IFFT/FFT Size Efficient Improved ACO-OFDM Scheme for Next-Generation Passive Optical Network," *European Conference on Networks and Optical Communications (NOC)*, Lisbon, pp. 111-116, 2016.
- [17] Z. Wang, T. Mao and Q. Wang, "Optical OFDM for Visible Light Communications," *International Wireless Communications and Mobile Computing Conference (IWCMC)*, Valencia, pp. 1190-1194, 2017.
- [18] S.M.Moser, "Capacity Results of an Optical Intensity Channel with Input-dependent Gaussian Noise," *IEEE Transactions on Information Theory*, vol.58, no.1, pp.207-223, Jan.2012.
- [19] A.Chaaban, J.Morvan, and M.Alouini, "Free-space Optical Communications: Capacity Bounds, Approximations, and a new Sphere-packing Perspective," *IEEE Transactions on Communications*, vol.64, no.3, pp. 1176-1191, Mar. 2016.
- [20] Gueymard, Chris, "SMARTS2, a simple model of the atmospheric radiative transfer of sunshine: algorithms and performance assessment," 1995.
- [21] B. Hussain, X. Li, F. Che, C. Patrick Yue and L. Wu, "Visible Light Communication System Design and Link Budget Analysis," *Journal of Lightwave Technology*, vol. 33, no. 24, pp. 5201-5209, 15 Dec.15, 2015

- [22] J. Duan, X. Wang, Y. Zhou, C. Wang and F. Grillot, "Carrier-Noise-Enhanced Relative Intensity Noise of Quantum Dot Lasers," *IEEE Journal of Quantum Electronics*, vol. 54, no. 6, pp. 1-7, Dec. 2018.
- [23] J. C. Cartledge and M. O'Sullivan, "Time- and Frequency-Domain Characterization of the Relative Intensity Noise of a Quantum-Dot Frequency Comb Source Laser," *IEEE Journal of Selected Topics in Quantum Electronics*, vol. 25, no. 6, pp. 1-9, Nov.-Dec. 2019.
- [24] H. J. Carmichael, "Spectrum of Squeezing and Photocurrent Shot Noise: a Normally Ordered Treatment," *Journal of Optical Society of America*, vol. 4, no. 10, pp. 1588-1603, Oct. 1987.
- [25] S. Donati, "Responsivity and Noise of Self-Mixing Photodetection Schemes," *IEEE Journal of Quantum Electronics*, vol. 47, no. 11, pp. 1428-1433, Nov. 2011.



Xu Li received the B.S. and Ph.D. degrees in electrical and electronics engineering from the University of Science and Technology of China (USTC), in 2010 and 2015, respectively. From 2013 to 2014, he was a Visiting Ph.D. student at the Department of Electrical Engineering and Computer Science, Northwestern University, U.S. His research involves various architectures of radio access network in 5G, especially the end to end network slicing. He has a rich wireless research experience including ultra-wide band (UWB) chips, interference alignment, relay networks, stochastic geometry, and public safety wireless broadband networks. His current research topics include microwave wireless communication, radio over fiber communication, and optical wireless communication.



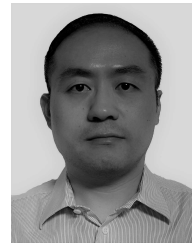
Jingjing Huang received the B.Eng. and M.S. degrees in electronic engineering from Tsinghua University, Beijing, China, in 2003 and 2006, respectively. After that he was admitted by University College London, UK and received his Ph.D. degree in electronic engineering in 2010. After graduation he joined Novella Satcomms in Leeds, UK and worked as a RF engineer for 2 years. In 2013 he joined Passive-Eye Ltd and developed a self-powering GPS tracking system. In 2015 he joined TP-Link technologies Co. LTD in Shenzhen, China and worked as a system engineer for one year. He is now with Huawei Technologies Co. Ltd and working at the Central Research Institute, 2012 Labs as a research engineer. His research interests include antennas, array signal processing, RF/microwave circuits, energy harvesting, low power wireless transceiver, backscatter communication, satellite communication and optical wireless communications.



Yibo Lyu received the M.Sc. degree in information and signal processing from the Chongqing University of Posts and Telecommunications in 2011 and the Ph.D. degree in circuits and systems from Xiamen University in 2016. His research interests include channel coding, joint source and channel coding, chaotic communications and nonlinear compensation. His current research projects including the modulation and coding methods for wireless optical communication system and the signal processing algorithms for radio over fiber system.



Rui Ni received the B.Sc. degree and Ph.D. degree in electrical and electronics engineering from University of Science and Technology of China, in 2006 and 2011, respectively. From 2011 to now, he was a principal engineer in the Central Research Institute, 2012 Laboratory of Huawei Tech. Co. Ltd. His research involves various architectures of radio access network and core network, such as LTE, UMTS, GSM, WiMAX and Wi-Fi. He has a rich communication network related experience in engineering practice. His current research interests include Beyond 5G, electromagnetic information theory, and new waveforms.



Jiajin Luo received the B.S. and M.S. degrees in electronic and communication engineering from Harbin Institute of Technology in 1999 and 2001, respectively. His research involves GNSS and indoor localization, satellite communication, cellular communication. He is experienced in system and signal design of GNSS, high dynamics signal acquisition and tracking, ultra-high sensibility receiver. His current research topics include positioning, integrated sensing and communication, joint communication and navigation.



Junping Zhang is a principal engineer of Huawei Wireless technology lab, Huawei, Shenzhen China. He is mainly engaged in optical wireless technology research and focuses on the application of optical spectrum in next-generation wireless communications. His research scope covers new optical sources, detectors, and new air interface technologies. He has more than 15 years of experience in wireless communications technology research and more than 20 granted patents.